IEEE Access
Multidisciplinary | Rapid Review | Open Access Journal

Received June 23, 2021, accepted July 8, 2021, date of publication July 14, 2021, date of current version July 22, 2021.

Digital Object Identifier 10.1109/ACCESS.2021.3097145

RF-Induced Heating of Various Tattoos at Magnetic Resonance Imaging Systems

SHAHZEB HAYAT[1], YOUNGDAE CHO[1], (Graduate Student Member, IEEE), SUKHOON OH[2], (Member, IEEE), AND HYOUNGSUK YOO[1], (Senior Member, IEEE)

[1]Department of Electronic Engineering, Hanyang University, Seoul 04763, Republic of Korea
[2]Center for Research Equipment, Korea Basic Science Institute, Cheongju 28119, Republic of Korea

Corresponding author: Hyoungsuk Yoo (hsyoo@hanyang.ac.kr)

This work was supported by the Institute for Information and Communications Technology Promotion (IITP) Grant by the Korean Government through the Ministry of Science, ICT and Future Planning (MSIP) (Development of precision analysis and imaging technology for biological radio waves) under Grant 2021-0-00490.

ABSTRACT This paper presents radiofrequency (RF)-induced heating of single and multiple tattoos during magnetic resonance imaging (MRI) at 1.5 T and 3 T. Various tattoos of different shapes, positions, pigment, length, diameter, and gap between the tattoos was investigated. Finite-difference time-domain based electromagnetic and thermal simulations were performed to study the specific absorption rate (SAR) and temperature rise, respectively. The results indicated that tattoos influenced the induced electric field distribution and maximum magnitude of the SAR on the surface of the skin. A notable enhancement in the SAR were observed around the sharp edges, long strips, and circular loops of tattoos. Interestingly, the maximum local SAR and increase in tissue temperature strongly depend on the shape of the tattoo. Furthermore, the relative position and size of the tattoos affected RF-induced heating. The RF-induced heating of multiple tattoos were investigated considering the worst case scenarios. Our results confirm that RF-induced heating of multiple tattoos is quite different from that of single tattoo and does not follow a simple superposition of the results from a single tattoos. Moreover, the procedures presented in the simulation environment are used to facilitate RF-induced heating for patients with tattoos undergoing clinical MRI.

INDEX TERMS Body coil, case study, electromagnetic simulations, MRI safety, RF heating, tattoos.

I. INTRODUCTION

Cosmetic and decorative tattoos have been of a topic of interest for decades worldwide. In the United States, permanent and cosmetic tattoos are used to recolor, recreate, and reshape eyebrows, lips, eyeliners, cheek blushes, and beauty marks [1]. The Food and Drug Administration (FDA) determines the ink used in tattoos and permanent makeup for cosmetic purposes. The pigments used in tattoo inks are color additives that require FDA and Cosmetic Act approval [2]. Therefore, the pigments used in tattoo inks for beauty applications have not been approved by the FDA owing to public health problems and safety issues [3]. Thus, occasional reports have been published on adverse reactions, including magnetic resonance imaging (MRI) complications [4]–[7].

MRI is a well-known imaging technique capable of producing high-quality images of the human body. MRI provides excellent multi-dimensional resolution without exposing patients to iodinated contrast agents or non-ionizing radiation [8]. Moreover, some safety issues are related to medical implanted devices (MID) undergoing MRI examination. When a patient with a MID undergoes MRI, the radiofrequency (RF)-induced energy generates localized energy, which causes increases the temperature near MIDs [9]. MIDs with long electrical leads are of great concern, such as deep brain stimulators or pacemakers, because the elongated lead picks up energy along its length which dissipated at the electrodes in the form of displaced current that can increase RF-induced heating in tissues [10]–[13]. A temperature increase of 0.6-15°C was observed around the pacemaker lead for 6 min MRI investigation [14]. Mattei *et al.* [15] investigated the RF-induced heating of metallic leads by measuring 375 configurations and demonstrated that the lead structure and location in the phantom are related to lead tip heating. Liu *et al.* [16] studied RF-induced heating of orthopedic implants with different dimensions and their locations in the human body. Their quantitative technique predicted that the RF-induced heating was strongly dependent on the

The associate editor coordinating the review of this manuscript and approving it for publication was G. R. Sinha.

implant size and location. Therefore, MRI is restricted for patients with MIDs because of safety concerns [17]–[21]. These safety concerns motivated us to investigate the safety of tattoos under MRI [22]. When patients with tattoo undergo MRI examination, adverse reactions (i.e., swelling, burning, and redness) occur due to the organic or metallic pigments found in the tattoo inks [5]. Thus, it is not surprising that the pigment from permanent tattoos might be influenced by the RF field during MRI.

There is a lack of detailed studies on clinical MRI examinations in tattooed patients. Relevant studies have shown that adverse effects of tattoos during MRI are uncommon; however, one study reported hazardous reactions in 1.5% cases with decorative and cosmetic tattoos [23]. Moreover, two cases of burn injuries in tattoo patients undergoing MRI examinations have been reported [24], [25]. In [24], a patient developed an inflammatory reaction with swelling erythema around a dragon tattoo with large circular loops and sharp edges on the neck and tail in the left thigh. Whereas in [25], a patient with a tattoo consisting of encircling Chinese symbols with two black jets developed a second-degree burn in the region of the deltoid. The burning sensation occurred around the two black jets and the thunderbolt in the tattoo. Furthermore, permanent makeup on the face, including eyeliner, eyebrow, blush, or lip liner, can cause similar problems [26]. The density of the skin tissue on the face is very low compared to that of other parts of the human body. Therefore, facial tattoos, permanent makeup, or pigment are not dispersed as deeply as other tattoos. The pigment tends to be closer to the surface of the skin, which can increase the risk of a burning sensation during MRI. Moreover, various symptoms ranging from stinging to burning sensations with premature termination of the session and warm feelings were reported in 2011-2012. In many studies, mild edema and redness around the tattoo were classified as cutaneous burns of ''grade I or II'' [27], [28]. To the best of our knowledge, cutaneous burns in tattooed patients with lesions on the skin and necrosis exposed to RF fields have not been studied in detail.

A significant challenge is the precise characterization of tattoo materials that may produce a burning sensation on the skin during an MRI examination. Several types of tattoo pigments are sensitive to magnetic fields, which can cause adverse effects in clinical events. Such effects may increase the temperature of tattoo pigments. A question arises whether individual color pigments or classes of tattoo pigments with certain physical behaviors or specific characteristics cause burning sensations. A literature review showed that ferromagnetic pigments (red, black, and brown) are more likely to cause the worst heating effects [29]. A few decades ago, the ''old-school'' tattoo style launched the dominant colorful and organic iron oxide pigments. These pigments have dull color tones and are commonly used in tattoo inks to prepare permanent makeup. Moreover, the risk of a burning sensation is especially high when metallic pigment (iron oxide) is organized in the form of sharp edges, multiple adjacent points, and large circular loops, as in the case of tattoo modeling [23].

The safety issues related to the possible interactions between the inks commonly used for tattoos, tattoo shape, and tattoo size and MRI electromagnetic (EM) fields should be further explored. Although some tattooed patients undergoing MRI have reported burning sensation during MRI or explicit mild swelling and erythema in the tattoo's proximity, [18] most tattooed patients do not report any noticeable consequences. The lack of knowledge about these safety implications may lead to a precautionary reaction from physicians, such as suggesting tattooed patients to avoid MRI. Despite the abundance of reported clinical cases of tattooed patients undergoing MRI examinations, there is a lack of systematic studies investigating the interaction between tattoo pigment, shape, size, and thickness and the RF field of MRI. To the best of our knowledge, this is the first study to model tattoos and quantitatively analyze their effects with different RF field strengths in MRI.

In this study, four types of tattoos were modeled. Numerical simulations with a realistic human body model (Duke) were performed to investigate the effect of RF-induced heating on different tattoo shapes. Simulations were performed at 1.5 T and 3 T with different tattoos at various positions of the body. We designed a 32-port MRI RF coil to investigate the effect of tattoos. The simulated results for tattoo loading, tattoo sizes, tattoo thicknesses, tattoo conductivities, and gaps between multiple tattoos were compared in terms of the peak spatial-average specific absorption rate (SAR) over 1-g of tissue. However, imaging studies were not included because of the presence of ferromagnetic or other magnetic materials in the tattoos.

This paper is organized as follows. The modeling of tattoos and computational methods are presented in section II. Section III present the corresponding results of tattoos with different types, position, size of tattoos, pigments, and multiple number of tattoos. The discussion and conclusion are presented in section IV and V, respectively.

II. METHODOLOGY

A. TATTOO DESIGN

Tattoos can hinder MRI depending on their size and shape and the pigment used in the tattoo. Owing to safety and health issues, the FDA has refused the approval of tattoo inks and pigments [2]. Therefore, it is necessary to investigate systematically the effects of tattoo under MRI. In this study, four different types of tattoos were modeled to investigate the corresponding increase in temperature and peak SAR near the skin surface. It should be noted that commercial and commonly used tattoos have complex structures and redesigning of the exact tattoos via simulations is not possible; however, an approximate model of the tattoo can be made. Celtic and tribal tattoos are commonly designed at various positions in the human body. For further clarification and detailed study, two simple tattoos (letter M and circle triangle) were considered. Generally, tattoos are made of different types of

TABLE 1. Detailed parameters of tattoos (units: millimeter).

M and Tribal Tattoo		Celtic Tattoo		Circle triangle Tattoo	
Parameter	Value	Parameter	Value	Parameter	Value
l_m	120	d_1 (ID)	140	r_1 (ID)	100
w	5	d_2 (OD)	160	r_2 (OD)	110
s_1	60	d_3 (ID)	140	l_1 (length)	88
s_2	60	d_4 (OD)	160	l_2 (length)	88
l_t	120	d_5 (ID)	210	l_3 (length)	88
w_t	40	d_6 (OD)	220	--	--

ID: Inner Diameter OD: Outer Diameter

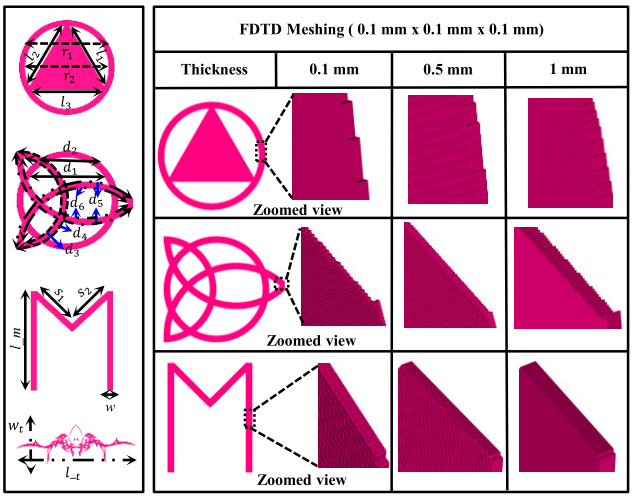

FIGURE 1. Overview of tattoo designs with various thicknesses. (a) Different tattoo designs. (b) Side view of tattoos with different thicknesses and the corresponding finite-difference time-domain (Fdtd) meshing with high grid resolutions.

organic, metallic, and non-metallic pigment [5]. In this study, a pure iron oxide pigment was used for all simulations, which has a higher electrical conductivity of 10^6 S/m [30], [31]. A detailed view of the proposed tattoos is shown in Fig. 1. Detailed parameters of the tattoos are listed in Table 1. The tattoos were placed on the back and neck of a realistic human phantom such that the tattoos cover the maximum area of skin. Various parameters of the tattoos were studied, as shown in Fig. 2. Each parameter (tattoo length, diameter, and its thickness) of different type of tattoos were studied on the basis of peak SAR over 1-g of tissue during MRI at 1.5 T and 3 T. Various conductivity values for iron oxide and the gap between the tattoos were considered to study the RF-induced heating of tattoos.

B. RF BIRDCAGE COIL

To obtain a uniformly distributed and circularly polarized B_1 field inside the RF coil, a high-pass birdcage coil was modeled for all simulations. The RF coil design used in this study is a generic coil with 32 ports and dimensions of 650 mm and 700 mm, as shown in Fig. 3(a). It consists of 16 equally

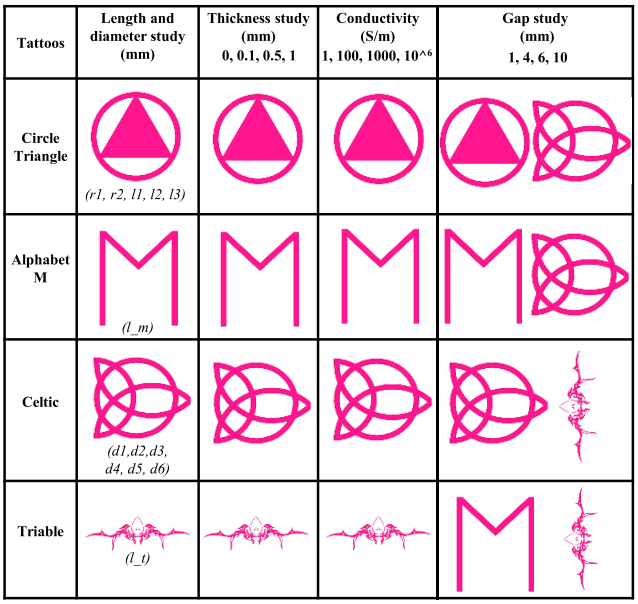

FIGURE 2. Investigation diagram of four different types of tattoos (rows) and four relatively independent parameter variations (columns). The numbers in each cell indicate the different parameters (length, diameter, thickness, conductivity, and gap).

spaced legs, 50 mm in width, and two end rings that form a circular shape. The RF coil has 32 sources on the upper and lower rings and does not have any lumped elements, as shown in Fig. 3(b). A voltage source was applied with an amplitude of 1 V and 50-Ω resistors in series. There was a successive phase delay of 22.5° between adjacent sources. For any two sources on the bottom and top ring at the same azimuthal position, the source on the top ring was advanced by 180° in phase. Fig. 3(c) presents the unloaded coil B_1 field distribution, in which the blue arrow indicates the B_1 field polarization direction at the center of the RF coil. B_1 is the principle component and is applied in the same manner in a clinical setting.

C. REALISTIC HUMAN BODY MODEL

The Duke model obtained from a virtual library population was used for all simulations [32]. The model is made up of 80 different types of tissues with a 1.5-mm cubical FDTD mesh size. The age, weight, and height of the model were 34 years, 70.2 kg, and 1.77 m, respectively. The given model was available with the commercial XFdtd base simulation software Sim4life which contains integrated moving, posing, morphing, and rotating tools. Parameters such as permeability, conductivity, and permittivity were assigned to the tissues at any desired frequency according to the ITIS database [26].

D. SIMULATION SETUP

All numerical simulations were conducted using the finite-difference time-domain method. The resonance frequencies of MRI were 64 MHz and 128 MHz at 1.5 T and 3 T, respectively. The absorbing boundary condition was applied

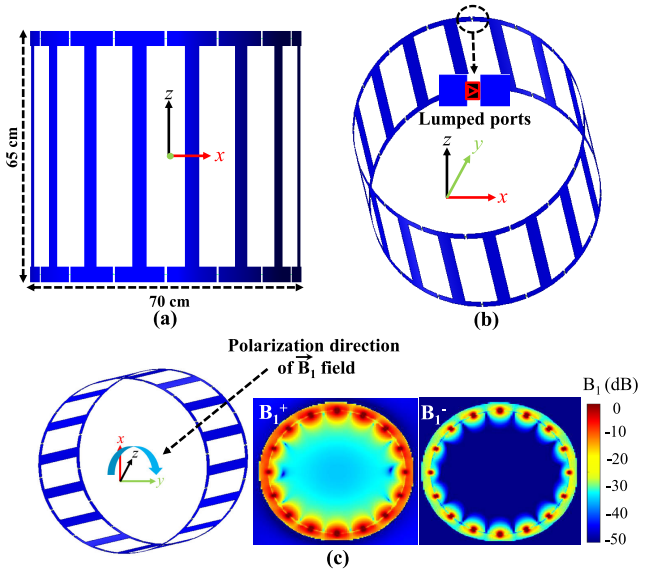

FIGURE 3. Overview of radio-frequency (RF) coil geometry. (a) Dimensions of the RF birdcage coil. (b) The RF birdcage coil has 32 lumped sources. (c) B1 field distribution of the RF birdcage coil.

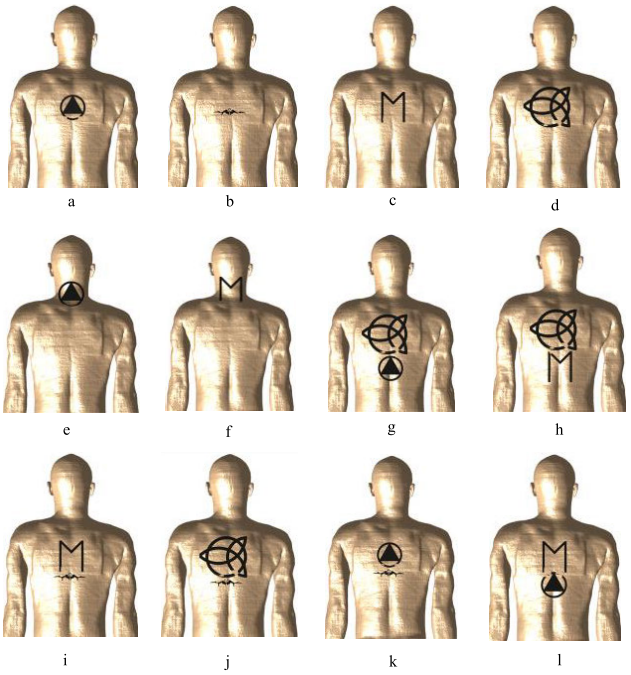

FIGURE 4. Overview of different types of tattoos on the human phantom. (a) Circle triangle, (b) Tribal, (c) Alphabet M, (d) Celtic, (e) Circle triangle on the neck, (f) Alphabet M on the neck, (g) Celtic and circle triangle, (h) Celtic and Alphabet M, (i) Alphabet M and tribal, (j) Celtic and tribal, (k) Circle triangle and tribal, and (l) Alphabet M and circle triangle.

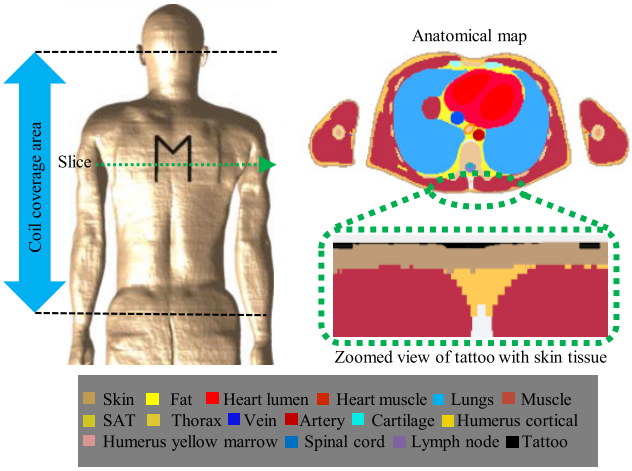

FIGURE 5. Positional relation between skin and tattoos.

in all six directions to reduce the simulation time. The simulation times were set to 30 periods to ensure convergence with an affordable computational burden. The voltage, currents, and E/H field were obtained after the simulation to ensure that the simulations converged. The maximum mesh steps were $1.5 \times 1.5 \times 1.5$ mm^3 for the human models. The grid resolution of $1 \times 1 \times 1$ mm^3 for tattoos was not sufficient to achieve optimum results. Therefore, a fine resolution of $0.1 \times 0.1 \times 0.1$ mm^3 was set for the tattoos. The human models were loaded in a series of positions along the z-direction. The initial positions of tattoos were at the center of the coil along the z-axis. Fig. 4 show the Duke model and the corresponding anatomical location of the tattoo in each exposure scenario. Furthermore, The positional relationship between skin tissues and tattoo pigment as shown in the Fig. 5.

Graphics processing unit hardware acceleration was achieved using CUDA solver with NVIDIA GTX 1070 GPU containing 8 GB memory. The 1-g SAR sensor is enabled to calculate the 1-g average SAR values within the skin tissues using the methods outlined by IEEE/IEC 62704-1 [33]. The 1-g average SAR was calculated over a volume surrounding each mesh point determined by the material's mass density to contain 1-g of mass. To quantify tattoo-induced SAR changes in the skin tissue, a maximum of 1-g was reported around the tattoos at 1.5 T and 3 T.

E. ELECTROMAGNETIC ENERGY DEPOSITION

RF-induced heating is closely related to the 1-g average SAR, which is defined as the energy absorbed by human tissue when exposed to an RF electromagnetic field. The standard SAR1g was proposed to compute RF-induced heating [34]–[36]. The SAR1g was calculated as follows [37]:

$$SAR = \sigma \mid E \mid^2 /2\rho, \tag{1}$$

where E is the magnitude of electric field, σ is the conductivity, and ρ is the mass density of biological tissue. Furthermore, the incident electric field (E_{inc} field) is responsible for inducing the RF currents on the conductive tattoos that eventually dissipate energy in the tissue and cause heating. The magnitude of tangential E-field ($\vec{E}_{tan}$) at each point is calculated as:

$$\vec{E}_{tan}(t) = \vec{E}(t) \times \vec{a}, \tag{2}$$

where $\vec{E}(t)$ and a is the incident field of the birdcage coil and normal unit vector, respectively.

F. THERMAL MECHANISM

The deposited EM energy around the tattoos can lead to a temperature rise in the lossy medium. Therefore, the temperature rise after RF field exposure was calculated in Sim4life by solving Penne's bio-heat equation [38]:

$$\rho c \frac{\partial T}{\partial t} = \nabla \cdot (k \nabla T) + \rho Q + \rho S - \rho_b c_b \rho \omega (T - T_b), \quad (3)$$

where c is the specific heat capacity of the skin; k is the isotropic thermal conductivity; ρ is mass density; T is the temperature; Q is the metabolic heat generation rate; t is the time; S is the SAR; ω is the blood perfusion rate; and c_b, T_b, and ρ_b are the specific heat, temperature of the blood, and density, respectively. The physical properties assigned to various materials at 128 MHz are summarized in Table 2.

TABLE 2. Physical properties of tissues and materials used in simulations.

Tissue	σ (S/ m)	ρ (kg/m^3)	ω_b (ml/100g/ min)	C (j/kg/ °C)	k (W/m/°C)	Q (W/m^3)
Blood	1.266	1057	100	3600	0.51	0
Fat	0.038	943	5	2300	0.498	758
Muscle	0.732	1070	5	3500	0.59	480
Skin	0.551	1125	12	3150	0.43	1125
Tendon	0.508	1151	12	3150	0.343	1125
Cortical bone	0.071	1850	1.4	1300	0.35	0

σ : Electrical Conductivity, ρ : Mass Density, ω_b : Perfusion by Blood, C : Heat Capacity, k : Thermal Conductivity, and Q : Metabolic Heat Generation

The region of interest for investigating the temperature rise had the same grid as that used for the EM simulation. The temperature rise was calculated by utilizing the thermal properties of tattoos and the time integration of the SAR1g. Thermal transient analysis was performed for 6 min, including the effect of blood perfusion. Dirichlet thermal boundary conditions were defined that correspond to normal breathing and clothing with little airflow. An accurate thermoregulation model is challenging and may be very specific to patients [39], [40]. In this study, the thermoregulation model proposed by Laakso and Hirata depended on the absolute temperature [41].

III. RESULTS

The RF-induced heating of tattoos and medical implants is considered a limiting factor when patients with tattoos or implants are examined under MRI. The EM distribution produced by the EM source might be changed around the tattoos as similar to the medical implants inside the human body [42]. Moreover, RF-induced heating depends on the resonance frequency, particular dimensions of the RF birdcage coil, patient posture, implant or tattoo location, and anatomy of the patient. Typically, several types of tattoos are placed at different positions on a Duke model to compute RF heating and increase in temperature around the tattoos. Simulations were performed for tattoos placed at different positions on an anatomical model, and partial SAR, whole-body, and local SAR were evaluated. The power loss must be averaged over the volume containing the 1-g of tissue. The maximum allowable input power was calculated based on the critical SAR aspect, which may exceed that proposed by the IEC guidelines [43]. Therefore, all the simulated results were normalized to the whole-body average SAR of 2 W/kg.

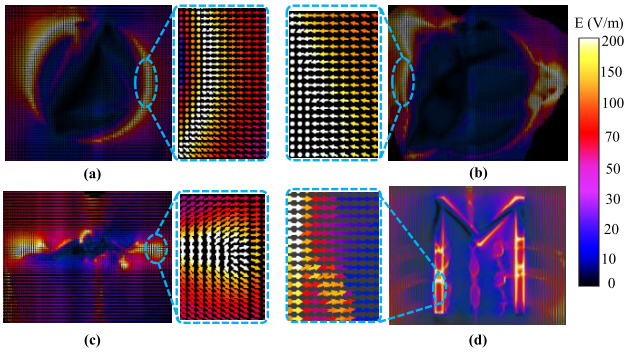

FIGURE 6. Distribution of induced E-field for tattoos due to tangential component of incident E-field that demonstrate 1-g SAR values at 1.5 T (a) Circle triangle, (b) Celtic, (c) Tribal, (d) Alphabet M.

A. INCIDENT ELECTRIC FIELD

In this study, we compare the orientation of the birdcage coil E_{inc} field along with different types of tattoo. The distribution of $\vec{E}_{tan}$ along the tattoos depend on the orientation of scattered E-field with respect to the different types as shown in Fig. 6. It can be observed from the figure that the electric field of the birdcage coil is orthogonally oriented to the tattoos. The RF birdcage coil has significant tangential component along different tattoos that induced a strong RF current on the sharp edges, long strip, and circular loops of tattoos. As can be seen from Fig. 6, the scattered E-field of the birdcage coil significantly influenced the long strip of alphabet M tattoo and sharp edges of tribal tattoo. Similarly, the scattered E-field is high on the large circular loops, sharp edges, and adjacent point of Celtic and circle triangle tattoos.

B. SIMULATION RESULTS OF SINGLE TATTOO AT 1.5 T AND 3 T

Different types of tattoo configurations were studied using a realistic model to explore the interactions of tattoos with the RF field during MRI. For diverse validation, different types of tattoos were placed on the back and neck of a realistic human phantom, as shown in Fig. 4. The peak 1-g average SAR values are given in Table 3 for different MRI field strengths. Possible clinical configurations, the types, and positions of tattoos were studied and the tattoo length, diameter, thickness, and gap were parametrically analyzed. Moreover, a parametric analysis of the iron oxide conductivity was performed. For safety concerns, the SAR should not be exceeded during an MRI examination. The 1-g SAR is commonly used to limit RF heating and provides information about the distribution of the electric field. Based on the numerical procedures described herein, each model was simulated with a 1.5 T and 3 T MRI body coil.

In the first step, the positions and shapes of the tattoo were investigated at the back and neck of the realistic model. Hot spots for the tattoos were identified on long strips, sharp edges, and multiple adjacent points of the tattoo. Based on a single tattoo, we analyzed how variation in the RF-induced heating depending on the shape of a tattoo. A comparison of the peak SAR1g on the coronal plane for different types of tattoos is shown in Fig. 7. It is clearly observed that the values of peak 1-g average SAR around the tattoos are influenced by the shapes of the tattoos at 1.5 T. The maximum EM energy absorption was observed close to the strip, adjacent points, circular loops, and sharp edges of the tattoos. As metallic tattoos are immersed in the RF field of the MRI, the induced E-field is coupled and scattered at the adjacent points, strips, and edges of the tattoos. Because of the mismatched impedance between the tattoos and skin tissue, additional scattered electric fields occur at different positions of the tattoos. Owing to ohmic loss in human tissues, energy is converted into heat, which increases SAR on the skin surface. The highest value of peak 1-g average SAR around the M tattoo was 38.6 W/kg. The worst case (the highest peak SAR near the tattoos) at 1.5 T occurs when a tattoo has a long strip or adjacent points that can easily absorb energy from the RF coil.

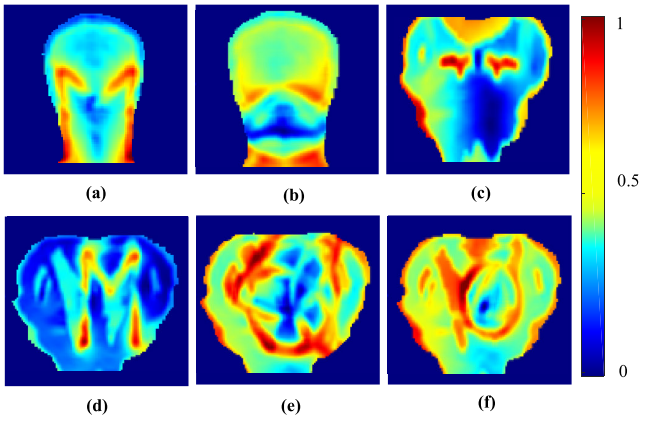

FIGURE 7. Comparison of normalized peak specific absorption rate (SAR) with different types of tattoos at 64 MHz. (a) Alphabet M on the neck, (b) Circle triangle on the neck, (c) Tribal, (d) Alphabet M, (e) Celtic, and (f) Circle triangle.

The results of RF-induced heating of tattoos according to the tattoo shape and position at different magnetic field strengths are shown in Fig. 8(a). The types and positions of tattoos affect the peak 1-g average SAR values around the tattoos near the surface of the skin at 3 T. The peak 1-g average SAR values around the long strips in M tattoos, sharp edges in Celtic and tribal tattoos, and adjacent points in circle triangle tattoos at 3 T were lower than those of 1.5 T with the same size and position of tattoos. The lower peak SAR1g at 3 T can be explained by the induced field strength on the tattoos. A higher energy loss was expected along the path from the realistic model to the tattoo at 3 T. Therefore, the scattered E-field on the tattoos at 3 T could be lower, which could lead to lower RF-induced heating. Moreover, the values of peak 1-g average SAR around tattoos are different because of the various scattered E-fields in the tattoo regions, which could vary RF-induced heating. Thus, the types (long strips, sharp edges, adjacent points, and circular loops) and positions of tattoos are very important factors that can affect RF-induced heating at 1.5 T and 3 T.

C. IMPACT OF TATTOOS LENGTH, DIAMETER, THICKNESS AND CONDUCTIVITY

The peak 1-g average SAR for all types of tattoos with different lengths, diameters, and thicknesses are shown in Fig. 8(b), 9(a), and 9(b), respectively. Computational results for all scenarios are summarized in Table 4.

In the first step, the lengths of M and tribal tattoos ranging from 80 mm to 140 mm were assessed at 1.5 T and 3 T. At 1.5 T, 140-mm M and tribal tattoos have the highest peak SAR. The increase in the current flow along the length of the M and tribal tattoos can easily absorb energy from the RF coil of MRI, which causes temperature increases and peak SAR on the surface of the skin. The M and tribal tattoos have the highest interaction with the MRI RF field because the lengths reached approximately a quarter wavelength at the resonance frequency. Therefore, strongly induced E-field variations or resonance effects are expected. Because of this resonance effect, the elongated structures of the M and tribal tattoos at 1.5 T have a higher heating effect compared to other tattoos, as shown in Fig. 8(b). Moreover, the increase in the length of these tattoos followed the same trend as for 1.5 T because elongated structures accumulated more RF fields compared to other tattoos at 3 T. The RF-induced heating effect is lower at 3 T for both tattoos with a length of 140 mm because of the lower interaction with the RF field. Furthermore, the diameter of the circle triangle tattoo ranged from 90 mm to 120 mm. The peak 1-g average SAR was observed around the adjacent points of the tattoos at 1.5 T and 3 T, as shown in Fig. 8(b). Moreover, the diameter of the Celtic tattoo ranged from 140 mm to 170 mm, which led to the highest peak SAR on the sharp edges and large circular loops at 1.5 T and 3 T, as shown in Fig. 8(b). The Celtic and circle triangle tattoos have notable effects on electric field distributions, particularly at the sharp edges and adjacent points of the tattoos. The length of tattoos had a high impact on RF-induced heating because of the greater interaction with the surrounding media of the different RF field strengths.

Iron oxide pigment contains different chemical classes, which have different electrical properties. Therefore, the conductivity of iron oxide was considered in the analysis of RF-induced heating. For parametric analysis, we chose different conductive values of iron oxide ranging from 1 to 10^6 S/m. Fig. 9(a) shows the variations in the peak SAR in the circle triangle and Celtic tattoos at 1.5 T and 3 T. The results showed a small variation in the peak SAR at different conductivities of iron oxide as shown in Fig. 9(a). Moreover, the partial loop with sharp edges increases the RF-induced heating compared to the circle triangle tattoo. This is due

TABLE 3. Simulated results of peak 1-g average SAR for different types of tattoos normalized to a whole-body SAR of 2 W/kg.

Exposure scenarios	Single tattoos		Length (l) and Diameter (d) (mm)								Thickness (mm)							
MRI systems	1.5 T	3 T	1.5 T				3 T				1.5 T				3 T			
l, d & Thickness	--		l_m, 80 l_t, 80 r2, 90 d2, 140	l_m, 100 l_t, 100 r2, 100 d2, 150	l_m, 120 l_t, 120 r2, 110 d2, 160	l_m, 140 l_t, 140 r2, 120 d2, 170	l_m, 80 l_t, 80 r2, 90 d2, 140	l_m, 100 l_t, 100 r2, 100 d2, 150	l_m, 120 l_t, 120 r2, 110 d2, 160	l_m, 140 l_t, 140 r2, 120 d2, 170	0	0.1	0.5	1	0	0.1	0.5	1
Circle triangle	5.24	6.30	3.24	4.45	5.24	6.56	4.65	5.56	6.3	6.96	5.24	5.56	6.32	6.98	6.3	6.78	7.23	7.98
Celtic	15.20	8.45	11.3	13.5	15.2	17.7	11.2	10.05	8.45	7.65	15.2	15.45	16.3	17.1	8.45	8.97	9.35	9.88
Tribal	21.5	15.9	17.6	20.35	21.5	25.6	11.5	13.5	17.5	15.32	21.5	21.98	22.68	22.96	15.9	16.34	16.85	17.25
M	34.6	19.0	23.6	26.1	34.6	48.8	11.5	12.5	19	16.5	34.6	34.9	35.3	36.02	19	19.45	19.95	20.43
Circle-neck	8.28	10.2	5.85	6.44	8.25	9.84	8.88	9.65	10.2	9.76	8.28	8.27	9.36	9.81	10.2	10.63	11.13	11.56
M-neck	32.5	15.3	25.6	27.65	32.5	36.2	11.8	12.96	15.3	13.55	32.5	32.89	33.41	33.86	15.3	15.84	16.32	16.68

l_m: M tattoo, l_t: triable tattoo, d2: Celtic tattoo, r2: circle triangle tattoo

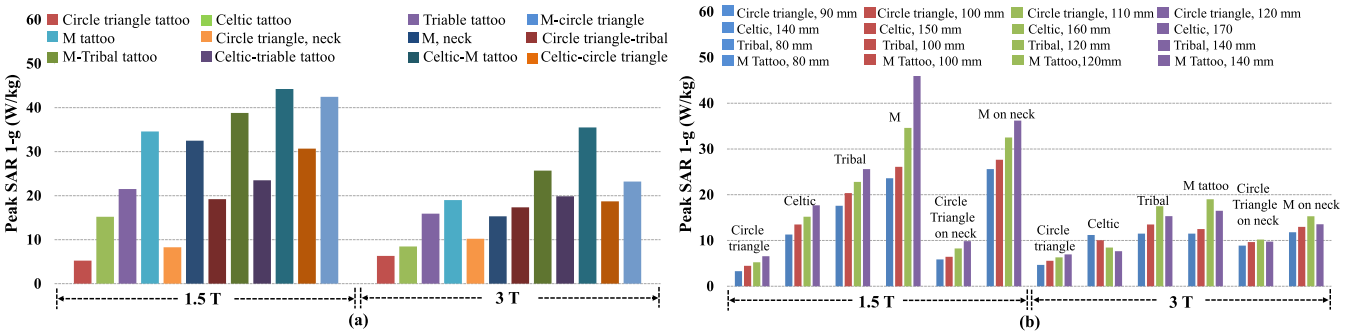

FIGURE 8. Summary of peak 1-g average specific absorption rate (SAR) results at 1.5 T and 3 T for different types of tattoos normalized to whole-body SAR of 2 W/kg. The graphs show the following variations: (a) peak 1-g average SAR of single and multiple tattoos and (b) the length and diameter of different types of tattoos.

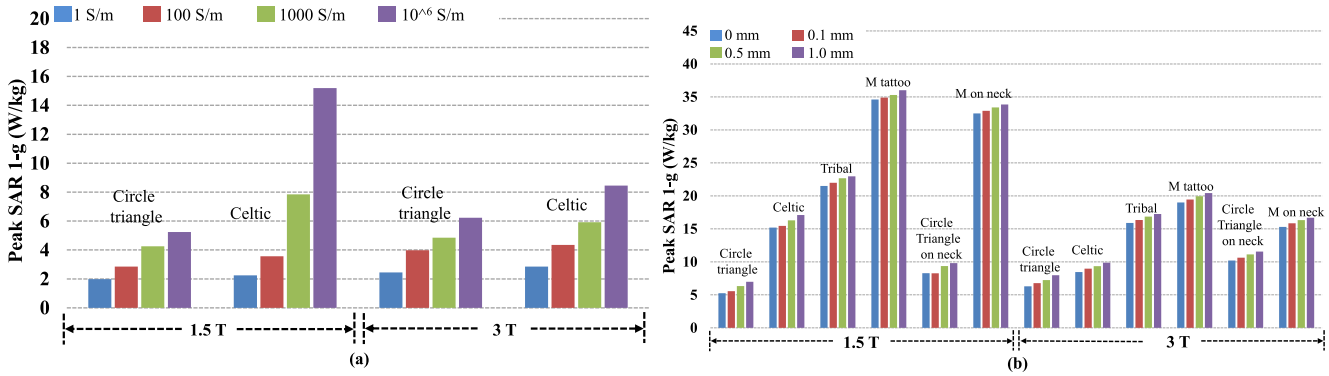

FIGURE 9. Summary of peak 1-g specific absorption rate (SAR) results at 1.5 T and 3 T for different types of tattoos normalized to whole-body SAR of 2 W/kg. The graphs show the following variations: (a) conductivity and (b) thickness of tattoos.

to the induced current around the partial loop and the sharp edges of the Celtic tattoo. The local SAR1g is proportional to the induced current and electrical conductivity of the lossy medium (skin tissue) surrounding the Celtic tattoo. Therefore, the RF-induced heating around the Celtic tattoo is higher than that around the circle triangle tattoos.

Typically, tattoos are located underneath the skin layer or the epidermis layer called dermis. Therefore, the thickness of tattoos has been considered in the study of RF-induced heating at different field strengths of MRI. The thickness of all tattoos ranged from 0 mm to 1 mm. Initially, tattoos were considered as a sheet with a default negligible thickness of 35 μm. Therefore, the negligible thickness was considered to be 0 mm in the simulation analysis. Fig. 9(b) shows that a small variation was observed in the RF-induced heating with increasing thickness of the tattoos at 1.5 T and 3 T. The energy depositions inside the Duke model along the tattoos with different thicknesses on the transverse plane are shown in Fig 10. It is clearly observed from the figure that M tattoos have less energy deposition on the skin tissues. Moreover,

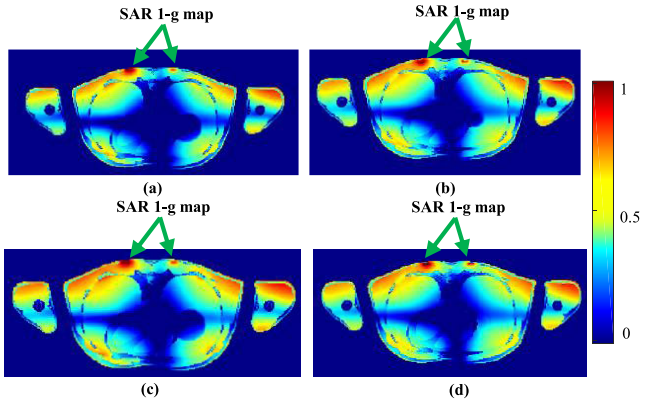

FIGURE 10. Comparison of normalized peak specific absorption rate (SAR) with different thickness of tattoos at 64 MHz (a) 0 mm (b) 0.1 mm (c) 0.5 mm (d) 1 mm.

the thickness of the tattoos had no significant impact on RF-induced heating. Therefore, the depth of tattoos with different thicknesses will lead to similar power dissipation along the path.

D. IMPACT OF MULTIPLE TATTOOS ON SAR AT 1.5 T AND 3 T

The multiple-tattoo configuration was studied to explore the difference between single and multiple tattoos, where the shape of the second tattoo was the same as that shown in Fig. 4. The highest peak SAR was observed for multiple tattoos compared to a single tattoo, as shown in Fig. 11. Furthermore, possible configurations of the tattoos and the gap between multiple tattoos were studied.

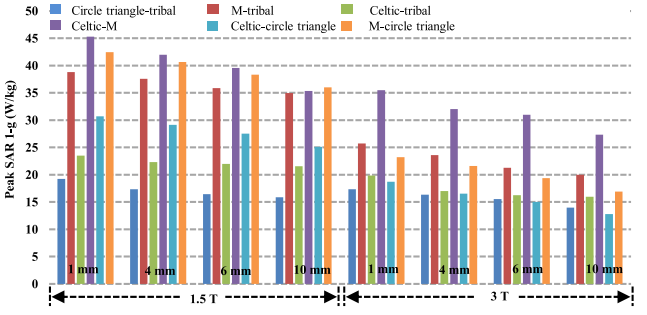

FIGURE 11. Summary of peak 1-g average specific absorption rate (SAR) results at 1.5 T and 3 T for different types of tattoos normalized to whole-body SAR of 2 W/kg. The graphs show the following variation: gap between multiple tattoos.

Initially, different types of multiple tattoos were closely spaced. In each case, the second tattoo was placed parallel to the first tattoo on the back side of the Duke model. For the gap study, the distance varied from 1 mm to 10 mm. Fig. 11 shows the variation in the peak 1-g average SAR according to the gap distance. The results showed that a small distance between tattoos could lead to a larger SAR for multiple tattoos because of the strong coupling of the RF field near the gap. When Celtic and M tattoos were closely spaced

TABLE 4. Simulated results of peak 1-g average SAR for different types of tattoos normalized to a whole-body SAR of 2 W/kg.

Exposure scenarios	Multiple tattoos		Gap (mm)							
MRI systems	1.5	3 T	1.5 T				3 T			
Gap (mm)			1	3	6	10	1	3	6	10
M-tribal	38.8	25.7	38.8	37.56	35.85	34.98	25.7	23.59	21.25	19.98
Celtic-tribal	23.5	19.5	23.5	22.32	21.98	21.54	19.85	17	16.22	15.95
Celtic-circle triangle	30.7	18.7	30.7	29.12	27.54	25.12	18.7	16.54	14.99	12.78
M-circle triangle	42.5	23.2	42.45	40.67	38.32	35.98	23.2	21.52	19.35	16.89
Circle triangle-tribal	19.2	17.35	19.2	17.35	16.45	15.87	17.35	16.32	15.54	13.98
Celtic-M	45.3	35.5	45.3	41.98	39.56	35.35	35.5	32	30.98	27.33

to each other with a distance of 1 mm, the peak 1-g average SAR values were larger at 1.5 T and 3 T compared with those for a single tattoo. The long strip of the M tattoo coupled with the sharp and circular loop of the Celtic tattoo could lead to maximum RF-induced heating at both field strengths of MRI. The results also showed that peak 1-g average SAR values for multiple tattoos with a 10-mm distance between them were larger than those for a single tattoo. Hence, the distance between tattoos is also an important factor to be considered in RF-induced heating. Table 4 summarizes the gaps between the tattoos at 1.5 T and 3 T.

In summary, RF-induced heating for multiple tattoos is, in most cases, higher than that for individual tattoos. The coupling effect between the two tattoos makes a positive contribution to the total electric field near the gap. Because the SAR is proportional to the square of the total electric field, the peak 1-g average SAR can be fairly large if the coupling effect induces a strong total electric field.

E. THERMAL SIMULATION FOR TEMPERATURE RISE

Based on similar SAR values, the temperature rise was calculated after 6 min of exposure to the MRI RF field using the bio-heat equation. A maximum temperature increase of 5.35°C was observed in the skin tissues that were in contact with long strips and the adjacent point of the M tattoo at 1.5 T. Hence, based on the thermal simulation results, we concluded that the temperature increase in the Duke model with different types of tattoos is unsafe under MRI. The final temperature increase observed in tattoo patients is presented in Table 5.

IV. DISCUSSION

The scattered E-field distribution around the tattoos differs according to tattoo type and position. RF-induced heating is different for different levels of absorbed RF energy. The distribution of the E_{inc} field may originate from the asymmetry of the Duke models with different dimensions along the x- and y-axes. The distributions of E-field strength on the x-y axis with and without the Duke model were extracted at 1.5 T and 3 T, as shown in Fig. 12. The distribution of the E-field is symmetrical on the y-axis without the Duke model

TABLE 5. Simulated temperature rise (°C) for different types of tattoos.

Exposure scenarios	MRI system		
Tattoos	Location	1.5	3 T
Without tattoos	---	0.6	0.8
Circle triangle	Back side	2.1	5.15
Celtic	Back side	4.9	6.97
Tribal	Back side	3.6	5.75
M	Back side	5.35	8.10
Circle-neck	Neck	3.96	6.96
M-neck	Neck	5.52	7.60
M-tribal	Back side	11.25	10.35
Celtic-tribal	Back side	9.56	8.32
Celtic-circle triangle	Back side	12.56	11.35
M-circle triangle	Back side	17.15	14.28
Circle triangle-tribal	Back side	13.98	11.75
Celtic-M	Back side	18.25	15.32

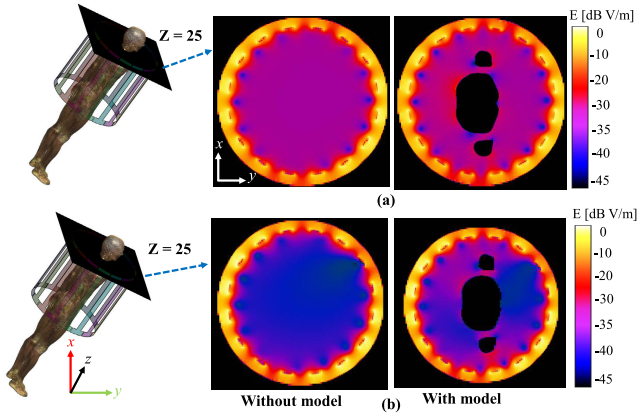

FIGURE 12. Electric field distributions in V/m with and without the loading of the Duke model. (a) 1.5 T and (b) 3 T.

at 1.5 T and 3 T. However, the distribution of the E-field changes by loading the Duke model in both RF fields. Thus, based on the types or positions of tattoos, the tattoos interact with different scattered E-field fields, leading to different RF-induced heating. The interaction between multiple tattoos (i.e., tattoo A and B for simplicity) is related to the scattering E-field. The magnitude of scattered E-field is presented in the following equation, which is related to SAR. When tattoos a and b are closely coupled to each other, the interaction of scattered E-field on both tattoos could be described as:

$$E^{tot}(r) = E^{inc}(r) + E^{A}_{sca}(r) + E^{B}_{sca}(r) + E^{A}_{B}(r) + E^{B}_{A}(r) + o(E^{sca}_{high}(r)), \quad (4)$$

where $E^{A}_{sca}(r)$ and $E^{B}_{sca}(r)$ are the first order scattered E-field of the tattoos A and B due to incident field generated by the MRI RF coil. $E^{A}_{B}(r)$ is the scattering E-field that is illuminated by the first order E-field of tattoo B. Similarly, $E^{B}_{A}(r)$ is the scattering E-field due to the first order E field of tattoo A. $E^{sca}_{high}(r)$ is the highest order scattering E-field that is less than first and second order terms.

The relationship between the electric field and SAR is cleared from equation 1 and 4. The average or local SAR value is high at the hot-spot position of tattoos, due to the existence of multiple tattoos that increased the scattered E-field, if it as in phase. Alternatively, the SAR could be reduced if the scattered E fields are out of phase.

We used a multiple tattoos as an example: The total E-field in the surrounding media is extracted at the same phase as depicted in the Fig. 13. The normal component of E-field exist at the surface of the tattoos and tangential E-field vanished because of the boundary conditions. As can be seen from the Fig. 13, most of E-field is in the same direction between the gap of the tattoos. Hence, when two tattoos are in close contact, the scattered E-field between the gap are in phase that can increase the total electric field. Therefore, high SAR was observed due to induced E-field between the gap of tattoos.

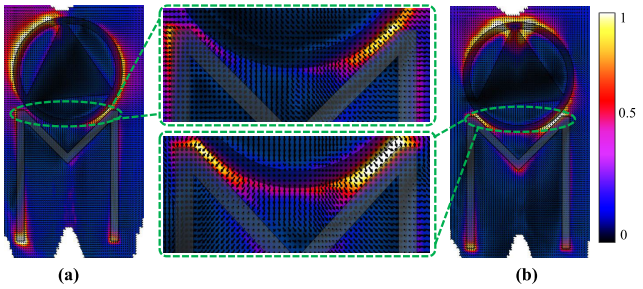

FIGURE 13. Electric field distributions of multiple tattoos with a gap of 3 mm. (a) 1.5 T and (b) 3 T.

In this study, numerical simulations using a realistic human model with different types and positions of tattoos were performed to study RF-induced heating effects. To mimic clinical MRI examinations, tattoo configurations with different types, positions, and conductivities of the tattoos were numerically investigated at 1.5 T and 3 T. The interaction of various types of tattoos is related to the scattered field. The local or peak SAR value is high because of the existence of sharp edges, multiple adjacent points, and long strips that increase the electric field. Moreover, the length and diameter of the tattoos strongly influenced RF-induced heating. The M and tribal tattoos had higher peak SAR values with increasing length owing to the strong interaction of the tattoos (long strips, adjacent points, and sharp edges) with the surrounding media of the RF field at 1.5 T. Similarly, for 3 T, the worst RF heating occurred with increasing lengths of M and tribal tattoos. In addition, a small variation in RF-induced heating was observed with increasing thickness of the tattoos. Furthermore, small variations were observed in the RF-induced heating effects around the tattoo owing to variations in the conductivity of iron oxide. Previous studies have reported that the ferromagnetic material found in the tattoo could lead to burning sensation during MRI examinations [4], [5], [23]. Our simulation results confirmed that the temperature increase and peak SAR are high when the iron oxide pigment is organized in the form of loops, adjacent points, sharp edges, and long strips.

This study only investigated four types of tattoos at two different positions on the human body for the initial analysis with RF the field of MRI. However, a more comprehensive study could be consider other metallic compounds found in tattoo pigments, different types of complex tattoos, imaging studies of ferromagnetic materials found in the tattoos, landmark positions, patient orientation, and tattoos located at different positions.

V. CONCLUSION

This study presents data regarding RF-induced heating around different types and positions of tattoos at different field strengths of MRI and investigated a substantial factors that may impact RF-induced heating. These factors include tattoo pigment, tattoo shape, tattoo thickness, multiple tattoos, gap between the tattoos, position of tattoos on a human phantom, and conductivity of iron oxide. The study reveals that tattoo shapes, and positions are the major factors that affect RF-induced heating during MRI. Furthermore, the size of the tattoos and the gap between multiple tattoos could lead to higher RF-induced heating at different field strengths of MRI. Moreover, tattoo thickness is associated with small variations in RF-induced heating. The radio frequency of MRI interacts with the ferromagnetic material found in tattoos, especially iron oxide. In addition, the RF-induced heating is different for different types of tattoos due to the different scattered E-fields. Thus, it is essential to study RF-induced heating in tattooed patients or follow the current recommendations of the FDA guidelines to avoid tattoo patient from MRI examination. Future studies on RF-induced heating of tattoos during MRI should consider patient orientation, landmark position, location of tattoos on the human body, tattoo pigments, and imaging studies.

REFERENCES

[1] W. D. Tope and F. G. Shellock, "Magnetic resonance imaging and permanent cosmetics (tattoos): Survey of complications and adverse events," *J. Magn. Reson. Imag.*, vol. 15, no. 2, pp. 180–184, Feb. 2002.

[2] US Food and Drug Administration. (2012). *Tattoos and Permanent Makeup: Fact Sheet*. Accessed: Jul. 1, 2015. [Online]. Available: https://www.fda.gov/cosmetics/cosmetic-products/tattoos-permanentmakeup-fact-sheet

[3] P. S. Islam, C. Chang, C. Selmi, E. Generali, A. Huntley, S. S. Teuber, and M. E. Gershwin, "Medical complications of tattoos: A comprehensive review," *Clin. Rev. Allergy Immunol.*, vol. 50, no. 2, pp. 273–286, Apr. 2016.

[4] N. Kluger, P. Brun-Lévêque, and N. Gral, "Painful burning sensation on a tattoo during magnetic resonance imaging," *Int. J. Dermatol.*, vol. 58, no. 4, pp. E82–E83, Apr. 2019.

[5] K. K. Alsing, H. H. Johannesen, R. H. Hansen, and J. Serup, "Tattoo complications and magnetic resonance imaging: A comprehensive review of the literature," *Acta Radiol.*, vol. 61, no. 12, pp. 1695–1700, Mar. 2020.

[6] D. Klitscher, J. Blum, K. F. Kreitner, and P. M. Rommens, "MRT-induzierte verbrennung bei Tätowierungen: Fallbericht eines unfallchirurgischen patienten," *Der Unfallchirurg*, vol. 108, no. 5, pp. 410–414, May 2005.

[7] S. Ratnapalan, M. Greenberg, and D. Armstrong, "Tattoos and MRI," *Amer. J. Roentgenol.*, vol. 183, no. 2, p. 541, Aug. 2004.

[8] R. Das and H. Yoo, "RF heating study of a new medical implant lead for 1.5 T, 3 T, and 7 t MRI systems," *IEEE Trans. Electromagn. Compat.*, vol. 59, no. 2, pp. 360–366, Apr. 2017.

[9] P. Serano, L. M. Angelone, H. Katnani, E. Eskandar, and G. Bonmassar, "A novel brain stimulation technology provides compatibility with MRI," *Sci. Rep.*, vol. 5, no. 1, p. 9805, Sep. 2015.

[10] M. Murbach, E. Zastrow, E. Neufeld, E. Cabot, W. Kainz, and N. Kuster, "Heating and safety concerns of the radio-frequency field in MRI," *Curr. Radiol. Rep.*, vol. 3, no. 12, p. 45, Dec. 2015.

[11] L. Winter, F. Seifert, L. Zilberti, M. Murbach, and B. Ittermann, "MRI-related heating of implants and devices: A review," *J. Magn. Reson. Imag.*, vol. 53, no. 6, pp. 1646–1665, Jun. 2021.

[12] E. Cabot, T. Lloyd, A. Christ, W. Kainz, M. Douglas, G. Stenzel, S. Wedan, and N. Kuster, "Evaluation of the RF heating of a generic deep brain stimulator exposed in 1.5 T magnetic resonance scanners," *Bioelectromagnetics*, vol. 34, no. 2, pp. 104–113, Feb. 2013.

[13] P. Nordbeck, I. Weiss, P. Ehses, O. Ritter, M. Warmuth, F. Fidler, V. Herold, P. M. Jakob, M. E. Ladd, H. H. Quick, and W. R. Bauer, "Measuring RF-induced currents inside implants: Impact of device configuration on MRI safety of cardiac pacemaker leads," *Magn. Reson. Med.*, vol. 61, no. 3, pp. 570–578, 2009.

[14] S. Pisa, G. Calcagnini, M. Cavagnaro, E. Piuzzi, E. Mattei, and P. Bernardi, "A study of the interaction between implanted pacemakers and the radio-frequency field produced by magnetic resonance imaging apparatus," *IEEE Trans. Electromagn. Compat.*, vol. 50, no. 1, pp. 35–42, Feb. 2008.

[15] E. Mattei, M. Triventi, G. Calcagnini, F. Censi, W. Kainz, G. Mendoza, H. I. Bassen, and P. Bartolini, "Complexity of MRI induced heating on metallic leads: Experimental measurements of 374 configurations," *BioMed. Eng. OnLine*, vol. 7, no. 1, p. 11, 2008.

[16] Y. Liu, J. Chen, F. G. Shellock, and W. Kainz, "Computational and experimental studies of an orthopedic implant: MRI-related heating at 1.5-T/64-MHz and 3-T/128-MHz," *J. Magn. Reson. Imag.*, vol. 37, no. 2, pp. 491–497, Feb. 2013.

[17] X. Ji, J. Zheng, R. Yang, W. Kainz, and J. Chen, "Evaluations of the MRI RF-induced heating for helical stents under a 1.5T MRI system," *IEEE Trans. Electromagn. Compat.*, vol. 61, no. 1, pp. 57–64, Feb. 2019.

[18] Q. Zeng, J. Liu, L. M. Angelone, T. Lloyd, S. Wedan, J. Chen, and W. Kainz, "Investigation of RF-induced heating near interventional catheters at 1.5 T MRI: A combined modeling and experimental study," *IEEE Trans. Electromagn. Compat.*, vol. 61, no. 5, pp. 1423–1431, Oct. 2019.

[19] A. R. Rezai, D. Finelli, J. A. Nyenhuis, G. Hrdlicka, J. Tkach, A. Sharan, P. Rugieri, P. H. Stypulkowski, and F. G. Shellock, "Neurostimulation systems for deep brain stimulation: *In vitro* evaluation of magnetic resonance imaging-related heating at 1.5 tesla," *J. Magn. Reson. Imag.*, vol. 15, no. 3, pp. 241–250, Mar. 2002.

[20] J. Zheng, X. Ji, W. Kainz, and J. Chen, "Study on search strategies for assessing the worst case RF-induced heating for multi-configuration implant system under MRI," *IEEE Trans. Electromagn. Compat.*, vol. 62, no. 1, pp. 43–51, Feb. 2020.

[21] M. Kozlov, W. Kainz, and L. Daniel, "Influence of metallic shielding on radio frequency energy-induced heating of leads with straight and helical wires: A numerical case study," *IEEE Trans. Microw. Theory Techn.*, vol. 68, no. 2, pp. 509–515, Feb. 2020.

[22] K. K. Alsing, H. H. Johannesen, R. Hvass Hansen, M. Dirks, O. Olsen, and J. Serup, "MR scanning, tattoo inks, and risk of thermal burn: An experimental study of iron oxide and organic pigments: Effect on temperature and magnetic behavior referenced to chemical analysis," *Skin Res. Technol.*, vol. 24, no. 2, pp. 278–284, May 2018.

[23] J. R. Ross and M. J. Matava, "Tattoo-induced skin 'burn' during magnetic resonance imaging in a professional football player: A case report," *Sports Health A, Multidisciplinary Approach*, vol. 3, no. 5, pp. 431–434, Sep. 2011.

[24] M. Vahlensieck, "Tattoo-related cutaneous inflammation (burn grade I) in a mid-field MR scanner," *Eur. Radiol*, vol. 10, no. 1, p. 197, Jan. 2000.

[25] W. A. Wagle and M. Smith, "Tattoo-induced skin burn during MR imaging," *Amer. J. Roentgenol.*, vol. 174, no. 6, p. 1795, Jun. 2000.

[26] M. L. Armstrong and L. Elkins, "Body art and MRI: Tattoos, body piercings, and permanent cosmetics may cause problems," *AJN, Amer. J. Nursing*, vol. 105, no. 3, pp. 65–66, Mar. 2005.

[27] T. Franiel, S. Schmidt, and R. Klingebiel, "First-degree burns on MRI due to nonferrous tattoos," *Amer. J. Roentgenol.*, vol. 187, no. 5, p. W556, Nov. 2006.

[28] K. M. Kuczkowski, "Lumbar tattoos, magnetic resonance imaging, and obstetric anesthesia: What do they have in common?" *J. Anesth.*, vol. 21, no. 2, p. 293, May 2007.

[29] M. L. Kreidstein, D. Giguere, and A. Freiberg, "MRI interaction with tattoo pigments: Case report, pathophysiology, and management," *Plastic Reconstructive Surgery*, vol. 99, no. 6, pp. 1717–1720, May 1997.
[30] L. Blaney, "Magnetite (Fe_3O_4): Properties, synthesis, and applications," Lehigh Univ., Bethlehem, PA, USA, Tech. Rep., 2007, vol. 15, p. 50.
[31] N. N. Greenwood and A. Earnshaw, *Chemistry of the Elements*. Oxford, U.K.: Butterworth-Heinemann, 1997, p.15.
[32] M. C. Gosselin, E. Neufeld, H. Moser, E. Huber, S. Farcito, L. Gerber, M. Jedensjö, I. Hilber, F. Di Gennaro, B. Lloyd, and E. Cherubini, "Development of a new generation of high resolution anatomical models for medical device evaluation: The virtual population 3.0," *Phys. Med. Biol.*, vol. 59, no. 18, p. 5287, Aug. 2014.
[33] P. A. Hasgall, F. D. Gennaro, and C. Baumgartner, "IT'IS database for thermal and electromagnetic parameters of biological tissues," Found. Res. Inf. Technol. Soc., ETH Zurich, Zürich, Switzerland, Version 4.0, Tech. Rep., May 2018. [Online]. Available: https://itis.swiss/virtual-population/tissue-properties/overview/, doi: 10.13099/VIP21000-04-0.
[34] *Draft Standard for Determining the Peak Spatial Average Specific Absorption Rate (SAR) in the Human Body From Wireless Communications Devices, 30 MHz-6 GHz. Part 1: General Requirements for Using the Finite Difference Time Domain (FDTD) Method for SAR Calculations*, Standard IEC/IEEE P62704-1, International Electrotechnical Commission/Institute of Electrical and Electronics Engineers, Geneva, Switzerland, Aug. 2016.
[35] S. M. Park, R. Kamondetdacha, A. Amjad, and J. A. Nyenhuis, "MRI safety: RF-induced heating near straight wires," *IEEE Trans. Magn.*, vol. 41, no. 10, pp. 4197–4199, Oct. 2005.
[36] F. G. Shellock, "Radiofrequency energy-induced heating during MR procedures: A review," *Magn. Reson. Imag.*, vol. 12, no. 1, pp. 30–36, 2000.
[37] E. R. Adair and R. C. Petersen, "Biological effects of radiofrequency/microwave radiation," *IEEE Trans. Microw. Theory Techn.*, vol. 50, no. 3, pp. 953–962, Mar. 2002.
[38] I. A. Shah and H. Yoo, "Assessing human exposure with medical implants to electromagnetic fields from a wireless power transmission system in an electric vehicle," *IEEE Trans. Electromagn. Compat.*, vol. 62, no. 2, pp. 338–345, Apr. 2020.
[39] M. Murbach, E. Neufeld, M. Capstick, W. Kainz, D. O. Brunner, T. Samaras, K. P. Pruessmann, and N. Kuster, "Thermal tissue damage model analyzed for different whole-body SAR and scan durations for standard MR body coils: Thermal dose and tissue damage in MR RF heating," *Magn. Reson. Med.*, vol. 71, no. 1, pp. 421–431, Jan. 2014.
[40] M. Murbach, E. Neufeld, T. Samaras, J. Córcoles, F. J. Robb, W. Kainz, and N. Kuster, "Pregnant women models analyzed for RF exposure and temperature increase in 3T RF shimmed birdcages," *Magn. Reson. Med.*, vol. 77, no. 5, pp. 2048–2056, May 2017.
[41] I. Laakso and A. Hirata, "Dominant factors affecting temperature rise in simulations of human thermoregulation during RF exposure," *Phys. Med. Biol.*, vol. 56, no. 23, pp. 7449–7471, Dec. 2011.
[42] I. A. Shah, Y. Cho, and H. Yoo, "Safety evaluation of medical implants in the human body for a wireless power transfer system in an electric vehicle," *IEEE Trans. Electromagn. Compat.*, vol. 63, no. 3, pp. 681–691, Jun. 2020.
[43] International Electrotechnical Commission (IEC), *Medical Electrical Equipment—Part 2-33: Particular Requirements for the Basic Safety and Essential Performance Edition 3.2*, document IEC 60601-2-33, 2015.

SHAHZEB HAYAT received the B.Sc. degree in telecommunication engineering from the University of Engineering and Technology, Mardan, Pakistan, in 2016. He is currently pursuing the M.S. degree leading to the Ph.D. degree in electronic engineering with the Applied Bioelectronics Laboratory, Hanyang University, Seoul, South Korea.

His current research interests include implantable antenna and systems, reconfigurable antenna, MRI and RF coils, implants and tattoos safety under MRI, intravascular catheter tracking under MRI, and intracranial catheter for drug delivery.

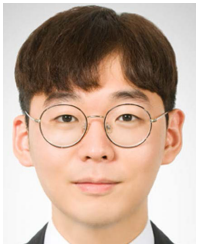

YOUNGDAE CHO (Graduate Student Member, IEEE) was born in Busan, South Korea, in 1993. He received the B.Sc. and M.S. degrees in biomedical engineering from the University of Ulsan, Ulsan, South Korea, in 2016 and 2018, respectively. He is currently pursuing the Ph.D. degree in electronic engineering with Hanyang University, Seoul, South Korea. His current research interests include implantable antennas and devices, wireless power transfer, magnetic resonance imaging and RF coils, and radio-frequency heating and safety. He was awarded the Second Prize for the Best Student Paper Competition 2016 by the Korea Communications Agency (KCA) and Korean Institute of Electromagnetic Engineering and Science (KIEES).

SUKHOON OH (Member, IEEE) received the B.Sc. degree in biomedical engineering from Konkuk University, South Korea, in 1998, and the M.Sc. and Ph.D. degrees in biomedical engineering from Kyung Hee University, South Korea, in 2002 and 2006, respectively. In 2006, he joined the Center for NMR Research, Pennsylvania State University, PA, USA, as a Postdoctoral Fellow. From 2008 to 2012, he was a Research Associate (full-time faculty) with the Department of Radiology, Pennsylvania State University. In 2012, he continued his research at New York University, NY, USA, as a Research Scientist, until he moved to Samsung Electronics, South Korea, in 2013. In Samsung Electronics, he participated development projects of 3T MRI system. Since 2016, he has been working with the Korea Basic Science Institute, South Korea, as a Senior Researcher. His research interest includes the RF safety assessments at high field MRI systems. For that, he has been conducting various EM field simulations, electric properties mapping, and MR thermometry experiments for an RF coils in the phantoms and *in-vivo*.

HYOUNGSUK YOO (Senior Member, IEEE) received the B.Sc. degree in electrical engineering from Kyungpook National University, Daegu, South Korea, in 2003, and the M.Sc. and Ph.D. degrees in electrical engineering from the University of Minnesota, Minneapolis, MN, USA, in 2006 and 2009, respectively.

In 2009, he joined the Center for Magnetic Resonance Research, University of Minnesota, as a Postdoctoral Associate. In 2010, he joined Cardiac Rhythm Disease Management, Medtronic, MN, USA, as a Senior Electromagnetic (EM)/MRI Scientist. From 2011 to 2018, he was an Associate Professor with the Department of Biomedical Engineering, School of Electrical Engineering, University of Ulsan, Ulsan, South Korea. He has been the CEO of ElectroMagnetics and Magnetic Resonance (E2MR), a startup company, since 2017. Since 2018, he has been an Associate Professor with the Department of Biomedical Engineering and the Department of Electronic Engineering, Hanyang University, Seoul, South Korea. His current research interests include EM theory, numerical methods in EMs, metamaterials, antennas, implantable devices, and magnetic resonance imaging in high-magnetic field systems.

Dr. Yoo was awarded the Third Prize for the Best Student Paper at the 2010 IEEE Microwave Theory and Techniques Society International Microwave Symposium.